Analysis of Special Problems in Continuously-Reinforced Concrete Pavements

WILLIAM ZUK, Associate Professor of Civil Engineering, University of Virginia, and Highway Research Engineer, Virginia Council of Highway Investigation and Research, Charlottesville, Virginia

In an attempt to fill gaps in the fundamental understanding of the behavior of continuously-reinforced concrete pavements, a number of studies on various topics are presented. Most are presented from a theoretical analytical viewpoint; but some, which are not readily adaptable to analysis, are presented from an experimental viewpoint. Some of the topics studied are pavement thickness, differences in behavior of deformed bars and plain wire mesh, buckling tendencies, horizontal and vertical alignment changes, end anchorage, crack behavior under repeated loading, and reduced slab rigidity due to cracks.

● ALTHOUGH continuously-reinforced highways pavements have been built in many states, the behavior of these pavements is still not fully understood. This is not to say, however, that the general behavior characteristics of why and how such a pavement functions under expansion and contraction are not known, for these facts have already been presented (1, 2, 3, 4, 5, 6, 7, 8, 9, 10, 11, 12). It is assumed that the general behavior of such pavements is already known, therefore only additional problems which heretofore have not been considered with any degree of thoroughness are discussed.

Aspects of the continuously-reinforced design discussed in this paper are the following:

1. Pavement thickness.
2. Comparison of behavior between deformed bars and plain wire mesh:
   (a) Percent steel.
   (b) Crack width.
3. Buckling tendency.
4. Movement on horizontal curves.
5. Movement on vertical curves.
6. Terminal anchorage configuration studies:
   (a) Strength.
   (b) Uplift.
7. Cracked slab behavior:
   (a) Reduced bending rigidity.
   (b) Increases in crack width under repeated loading.

Topics 1 through 5 are studied from a theoretical mathematical standpoint, which affords the advantage of generality but is, of course, limited by the validity of the initial assumptions made. General field observations have, however, shown the legitimacy of most of these assumptions.

Topics 6 and 7 are discussed through experimental laboratory data. An attempt is made in the discussion of these experimental tests to indicate the fundamental reasons and trends in such a way that reliable general conclusions may be obtained from them.

PAVEMENT THICKNESS

As shown by Vetter (13), the amount of reinforcing steel necessary in pavements is controlled by such changes in the pavement as shrinkage, moisture-induced swelling, and temperature. In contrast, the thickness of the pavement is controlled by the wheel loads. Westergaard's theories (14) are not entirely applicable in continuously-reinforced pavements, as such pavements have innumerable closely-spaced transverse cracks

requiring a new approach to analysis based on cracked-slab behavior, rather than on homogeneous behavior.

Bending

Consider a long slab of thickness t, of width l, with transverse cracks closely spaced at a distance of b, which is assumed small in comparison with l (Fig. 1). Inasmuch as the concrete between cracks is still essentially homogeneous, this portion of slab is extracted as a free body and used as the basis of analysis in accordance with Figure 2, in which

K_1 is the elastic subgrade modulus per width b;
K_2 is the elastic restraint modulus of the adjacent segments transferred by the longitudinal steel; and
K_3 is the aggregate interlock modulus (assumed linear);

The differential equation of behavior of this slab segment is

$$D\frac{d^4 y}{dx^4} + K y = 0 \qquad (1)$$

in which

$$D = \frac{E_c b t^3}{12}; \qquad (2)$$

$$K = K_1 + K_2 + K_3; \qquad (3)$$

E_c = modulus of elasticity of concrete; and

y = deflection.

The wheel load is positioned at the end to produce the maximum bending moment. The weight of the slab is neglected. The solution to Eq. 1 is

$$y = \frac{2P\beta}{K(\sinh^2 \beta l - \sin^2 \beta l)}$$

$$\left[\sinh \beta l \cos \beta \cosh \beta (l-x) \right.$$

$$\left. \sin \beta l \cosh \beta \cos \beta (l-x)\right] \qquad (4)$$

in which

$$B = \sqrt[4]{\frac{K}{4D}} \qquad (5)$$

The maximum bending moment, $D\left[\frac{d^2 y}{dx^2}\right]_{max}$, occurs near the end and is equal to

$$M_{max} = 0.32\frac{P}{\beta} \qquad (6)$$

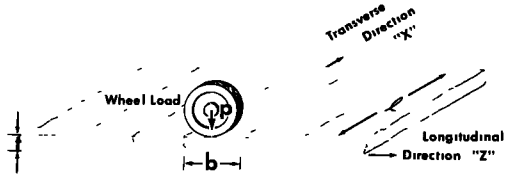

Figure 1. Cracked continuously-reinforced pavement.

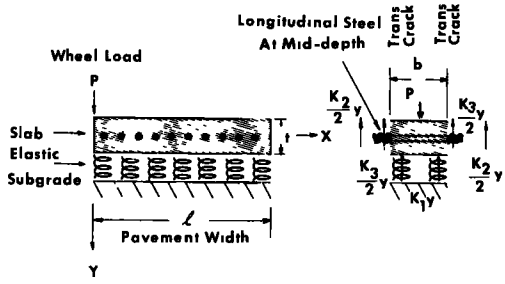

Figure 2. Slab segment.

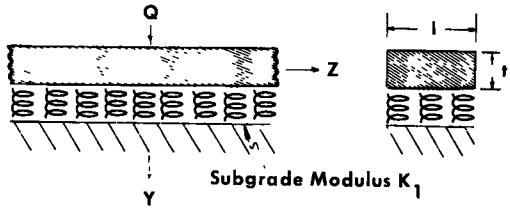

Figure 3. Longitudinal strip.

If the concrete is not to crack in bending, from simple homogeneous beam theory:

$$M_{max} = f_t \left[\frac{b\,t^2}{6}\right] \tag{7}$$

in which f_t is the allowable tensile stress of concrete. Thus, substituting for M_{max} and β, and solving for allowable thickness t based on bending:

$$t = \left[\frac{4.526\,E_c\,P^4}{(f_t)^4\,b^3\,(K_1 + K_2 + K_3)}\right]^{\frac{1}{5}} \tag{8}$$

The subgrade modulus, K_1, may be obtained from tests for small deflections. The aggregate interlock modulus may also be obtained from tests. Information on this value is lacking at present, but it is assumed to be dependent on the crack width. For a conservative analysis K_3 may be neglected. The value of K_2, the elastic restraint modulus, however, may be obtained semi-analytically in the following manner.

Consider a long segmented strip of slab in the longitudinal direction, of thickness t and of unit width. Note that this strip is not homogeneous, as it has transverse cracks. Extract this strip and consider it as a free body, as in Figure 3.

By inspection, the modulus K_2 may be defined as

$$K_2 = \frac{Q}{\delta_q} \tag{9}$$

in which Q is any load and δ_q is the deflection at the load Q. δ_q may be obtained from the differential equation

$$D_r \frac{d^4y}{dz^4} + K_1' y = 0 \tag{10}$$

for y at z = 0. Thus,

$$\delta_q = \frac{Q\,\beta 1}{2\,K_1'} \tag{11}$$

in which

$$\beta_1 = \sqrt[4]{\frac{K_1'}{4\,D_r}} \tag{12}$$

$$K_1' = \frac{K_1}{b} \tag{13}$$

$$D_r = \frac{E_r\,t^3}{12\,(1-\mu^2)} \tag{14}$$

μ = Poisson's ratio for concrete; and
E_r the reduced modulus of elasticity for cracked reinforced concrete (see section on, "Cracked Slab Behavior").

Therefore, upon substitution of these values

$$K_2 = \frac{2K_1'}{\sqrt[4]{\frac{K_1'}{4\,D_r}}} = \frac{2K_1}{b\sqrt[4]{\frac{K_1}{4\,b\,D_r}}} \tag{15}$$

Shear

For design use, a trial value of pavement thickness t may be had from Eq. 8, derived on the basis of bending. The slab should also be checked for shear or diagonal tension. Considering the same slab segment as in Figure 1, the critical position of load P for shear is also at the edge. Figure 4 shows the action of the essential forces, neglecting bending stresses.

From equilibrium of forces in the Y direction,

$$P - b(K_1 + K_2 + K_3)\int_0^t y\,dx - b\,t\,f_t = 0 \tag{16}$$

Thus, the allowable tension stress is controlled by

$$f_t = \frac{P}{bt} - \frac{(K_1 + K_2 + K_3)}{t}\int_0^t y\,dx \tag{17}$$

The value of y may be had from Eq. 4 or from published curves and tables found in such texts as "Strength of Materials II," by Timoshenko, or "Advanced Mechanics of Materials," by Seely and Smith, under the subject of beams on elastic foundations.

Example

As a numerical example of design, consider the following values:

$E_c = 3\text{x}10^6$ psi; $f_t = 90$ psi; b = 6 in. (assumed as tire contact length for limiting case); P = 12,000 lb; $K_1 = 10{,}000$ psi; $K_3 = 1{,}000$ psi; $E_r = 4{,}000$ psi; and $\mu = 0.225$.

Assuming a trial t=6 in., K_2 computed from Eq. 15 is 12,200 psi. t based on bending may then be computed from Eq. 8 as 6.07 in.

The allowable tensile stress f_t is next checked from Eq. 17 to be 121 psi. Because this exceeds the allowable stress of 90 psi, the trial thickness of 6.07 in. is too small. A revision based on Eq. 17 then increases the slab thickness to 6.7 in.

In practice, this thickness would probably be evened off to 7 in. Several continuous pavements of 7-in. thickness have been built in Illinois and have performed well in five years of service (15). This example problem is not intended to be used as a design criterion, but is presented simply to show the use of the basic equations.

This method of analysis for determining the pavement thickness thus provides a rational basis for determining the slab thickness. Certain refinements are still needed in the more complete understanding of the aggregate interlock force and reduced slab rigidity, both of which enter the slab thickness problem.

COMPARISON OF BEHAVIOR BETWEEN DEFORMED BARS AND PLAIN WIRE MESH

To simplify the comparison of deformed bars and plain wire mesh as much as possible, only their behavior in connection with shrinkage of concrete is discussed.

The basic behavior of deformed bars has been studied (13), so that only the behavior of plain welded wire mesh need be studied in this paper. However, to assist in the comparison, a summary of Vetter's results is presented for deformed bars.

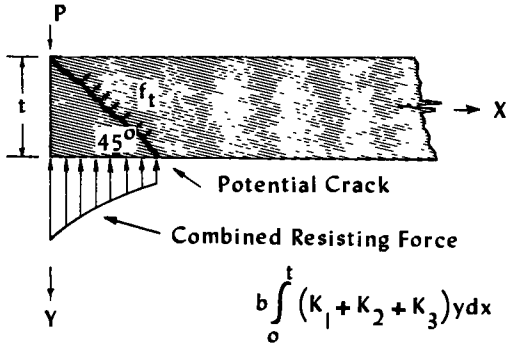

Figure 4. Diagonal tension.

Percent Steel for Deformed Bars

Vetter (13) showed that when reinforced concrete cracks due to shrinkage, the shrinking concrete grips the steel by bond in an extended region near the cracks, causing the concrete to go into tension. The bond force is assumed uniform in the region of grip near the cracks and zero in the central region between cracks. Tests have shown this to be a valid assumption. This action causes the steel near the cracks to go into tension and causes the steel in the central region between cracks to go into compression. For comparison studies it is important to stress the fact that the concrete slips a little in the region of the bond; but since the bars are deformed, bond forces continue to be developed.

Vetter found that for no shrinkage cracks to develop in reinforced concrete, the limiting value of the shrinkage coefficient z must be S'_c/E_c, in which S'_c is the tensile strength of concrete.

The limiting percentage of steel is found as

$$p = \frac{S'_c}{S_c + z E_s - n S'_c} \tag{18}$$

in which

$$p = \frac{A_s}{A_c} = \frac{\text{area of steel}}{\text{area of concrete}};$$

S_s = Elastic limit of steel;

E_s = Modulus of elasticity of steel; and

$n = E_s / E_c$.

The crack spacing L is found as

$$L = \frac{(S'_c)^2}{n p^2 q u(z E_c - S'_c)} \tag{19}$$

in which

$q = \Sigma_0 / A_s = \frac{\text{perimeter of bar}}{\text{area of steel}}$, and u is unit bond stress.

Percent Steel for Plain Welded Wire Mesh

A complete understanding of the exact bond behavior of wire mesh is not yet known, but based on bond tests by Anderson (16), the following statements appear reasonable. The primary "bond" behavior is really an anchorage behavior, where instead of bond being distributed along the wire (as in the case of deformed bars), it is concentrated at discrete anchorage points where the transverse wires intersect the longitudinal wires. An anchorage strength as strong as the strength of the main steel is achieved for transverse wire sizes not smaller than 4 or 5 wire sizes below that of the main wire size. This means that most of the force exerted on the longitudinal wire is transferred to the concrete through the first transverse wire intersection in the line of action of the force. Furthermore, it is believed that at this ultimate strength any small amount of adhesive bond existing between the concrete and the main wire between the anchorage points is broken by virtue of slip.

Therefore, in the analysis to follow no distributed bond is considered, and all "bond" is assumed concentrated at the first transverse wire intersection nearest a crack in the concrete. Only shrinkage action is assumed to take place. Subgrade frictional forces are neglected, as the real movement of the concrete in contact with the subgrade is quite small. Tests by Friberg (1) have shown that a movement of about 0.1 in. is required before appreciable subgrade friction can develop. The analysis is also limited to the

central region of a continuously-reinforced pavement, where no over-all changes in length occur in the steel.

Referring to Figure 5, m is an even integer, A_s is the area of steel, and A_c is the area of concrete. Under the initial assumption that the over-all steel length is unchanged,

$$\frac{T_s\, d}{A_s\, E_s} - \frac{C_s\,(m\, d)}{A_s\, E_s} = 0 \tag{20}$$

This reduces to

$$f_s = m\, f'_s \tag{21}$$

in which f_s is the tensile stress of steel and f'_s is the compressive stress of steel. Because the first transverse wire from the crack carries the anchorage force, between these terminal wires the compressive deformation of the steel must equal the net elongation of the concrete.

$$\frac{C_s(m\, d)}{A_s\, E_s} = z(m\, d) - \frac{T_c(m\, d)}{A_c\, E_c} \tag{22}$$

This reduces to

$$C_s = A_s\, E_s\, z - p\, n\, T_c \tag{23}$$

Substituting Eq. 23 in Eq. 20 and reducing gives

$$f_s = m(E_s\, z - n\, f'_c) \tag{24}$$

or

$$m = \frac{f_s}{E_s\, z - n\, f'_c} \tag{25}$$

where f'_c is the tensile stress in the concrete.

An additional relationship may be obtained from equilibrium of forces at the anchorage:

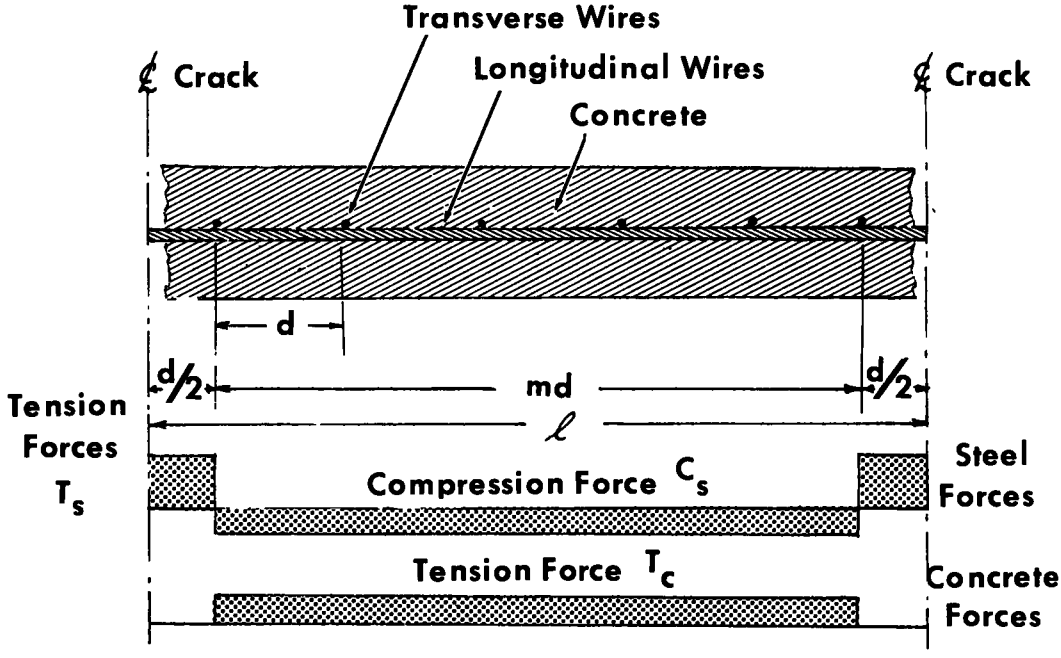

Figure 5. Wire mesh.

$$C_s + T_s = T_c \tag{26}$$

or, in terms of stresses,

$$A_s f'_s + A_s f_s = f'_c A_c \tag{27}$$

Using Eq. 21,

$$f_s = \frac{m f'_c A_c}{A_s + m A_s} \tag{28}$$

Equating Eqs. 24 and 28 and solving for m gives

$$m = \frac{A_s n f'_c + f'_c A_c - A_s E_s z}{A_s E_s z - A_s n f'_c} \tag{29}$$

Thus,

$$L = m d = \frac{A_s n f'_c + f'_c A_c - A_s E_s z}{A_s E_s z - A_s n f'_c} d \tag{30}$$

Note that for no cracks to develop, $L = \infty$, so that the denominator of Eq. 30 equals zero;

$$A_s E_s z - A_s n f'_c = 0 \tag{31}$$

or

$$z_{\text{lim for no cracks}} = S'_c / E_c \tag{32}$$

which is the same as Vetter (13) found for slabs reinforced with deformed bars.

To obtain the minimum percentage of steel so that the tensile stress in the concrete will be at its limit of S'_c and the tensile stress in the steel will be at its elastic limit of S_s, set $f'_c = S'_c$ and $f_s = S_s$ in Eqs. 25 and 28 and substitute Eq. 25 in Eq. 28:

$$P_{min} = \frac{S'_c}{S_s + z E_s - n S'_c} \tag{33}$$

The crack spacing for p_{min} may be found from Eq. 25 to be

$$L = d(m + 1) = d \left(\frac{S_s}{E_s z - n S'_c} + 1 \right) \tag{34}$$

It should be noted that the equation for the minimum percentage of steel for slabs reinforced with wire mesh is the same as for slabs reinforced with deformed bars as found by Vetter (13).

It may be of interest to point out in the analysis that the crack spacing L, and consequent steel stress, represent a limiting case on the conservative side. It is entirely possible that through certain regularities or irregularities in the concrete, cracks may form at smaller distances than indicated by Eq. 30. Indeed, cracks could even form near every transverse wire. Assuming no adhesive bond of the plain wire in this case, the concrete will merely crack at an interval d whenever z reaches S'_c / E_c, and the steel stress and concrete stress will both be zero. It is thus seen from this discussion that crack spacing and steel stresses may be predicted within maximum and minimum limits.

Crack Width for Deformed Bars

Under the operating assumptions established, it is seen that there is no distinction in behavior between deformed bars and wire mesh in regard to amount of steel. However, there is a significant difference in crack spacing and crack width. Consider deformed bars first. Vetter (13) showed the stress in the concrete to be as shown in Figure 6. He found the bond length to be

$$x = \frac{A_c f'_c}{u \Sigma_0} \tag{35}$$

The crack width at the steel due to slippage of the concrete is thus

$$W_1 = z\,L - \frac{1}{E_c}\int_0^L f_t\,dL \tag{36}$$

where f_t is the tensile stress of the concrete.

Integrating Eq. 36 and reducing gives

$$W_1 = z\,L - \frac{f'_c}{E_c}\left(L - \frac{A_c\,f'_c}{u\,\Sigma_0}\right) \tag{37}$$

Thus, for p_{min}

$$W_1 = zL - \frac{S'_c}{E_c}\left(L - \frac{A_c\,S'_c}{u\,\Sigma_0}\right) \tag{38}$$

To study the question of the variation of crack width at the steel and at the surface of the concrete, as shown in Figure 7, the following analysis is presented.

If the longitudinal steel is considered to be close together, the concrete behavior may be considered as two-dimensional and the planar methods of the mathematical theory of elasticity may be used. Deduced from Figure 6, the shrinkage forces on the concrete are as shown in Figure 8.

The Airy stress function for this case has been published by Winter (17). After a slight modification in the constant K_n to fit the conditions of the present problem, this stress function is

$$\phi = \sum_{n=1,2,3}^{\infty} (A_n \cosh a_n y + B_n \sinh a_n y + C_n y \cosh a_n y + D_n y \sinh a_n y) \cos a_n x \tag{39}$$

in which

$$a_n = \frac{n\pi}{2l} \tag{40}$$

$$A_n = -K_n \frac{\sinh^2 a_n b + (a_n b)^2}{a_n^2 (\sinh 2a_n b + 2a_n b)} \tag{41}$$

$$B_n = \frac{K_n}{2a_n^2} \tag{42}$$

$$C_n = \frac{K_n}{2a_n} \tag{43}$$

$$D_n = -K_n \frac{\cosh^2 a_n b + 1}{a_n(\sinh 2a_n b + 2a_n b)} \tag{44}$$

$$K_n = \frac{2\,A_c\,S'_c}{n\,L} \sin\frac{n\pi}{4} \tag{45}$$

First, from this stress function (Eq. 39) the exact distribution of stress may be

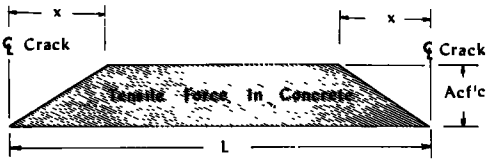

Figure 6. Concrete force.

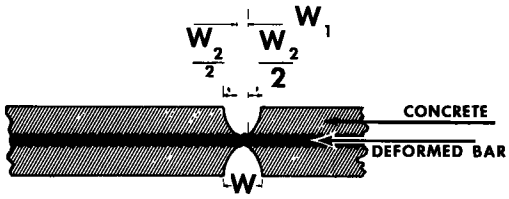

Figure 7. Crack shape.

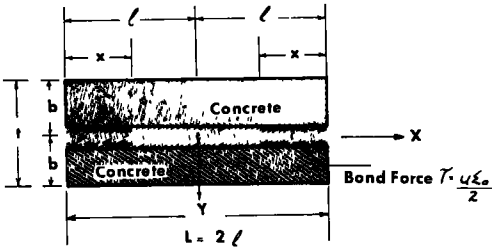

Figure 8. Boundary forces.

found in the concrete from the established principles of elasticity. That is, the longitudinal stress σx at any point in the concrete at coordinates x and y may be found by

$$\sigma x = \frac{\delta^2 \phi}{\delta y^2} \tag{46}$$

Thus,

$$\sigma x = \sum_{n=1,2,3}^{\infty} (A_n a_n^2 \cosh a_n y + B_n a_n^2 \sinh a_n y + C_n a_n^2 y \cosh a_n y + 2C_n a_n \sinh a_n y + D_n a_n^2 y \sinh a_n y + D_n a_n \sinh a_n y + D_n a_n \cosh a_n y) \cos a_n x \tag{47}$$

A study of Eq. 47 reveals that the stress near the surface of the concrete is less than that near the steel and also that the stress near the outside corners is very small.

With the exact stress distribution known, the increase in crack width at the surface over that at the steel may be found as:

$$W_2 = 2 \left[(W')_{y=0} - (W')_{y=b} \right] \tag{48}$$

Neglecting Poisson's ratio,

$$(W')_{y=0} = \frac{1}{E_c} \int_0^l (\sigma x)_{y=0} \, dx \tag{49}$$

$$(W')_{y=b} = \frac{1}{E_c} \int_0^l (\sigma x)_{y=b} \, dx \tag{50}$$

After carrying out these operations, W_2 from Eq. 48 becomes

$$W_2 = \frac{2}{E_c} \sum_{n=1,2,3}^{\infty} \left(B_n + \frac{C_n - \psi n}{a_n} \right) \sin a_n l \tag{51}$$

in which

$$\psi n = (B_n a_n^2 + 2 C_n a_n + D_n a_n^2 b + D_n a_n) (\sinh a_n b) + (A_n a_n^2 + C_n a_n^2 b + D_n a_n) (\cosh a_n b) \tag{52}$$

Crack Width for Wire Mesh

From Figure 5 it is clear that the crack width at the steel is

$$W_1 = z d + \frac{T_s d}{A_s E_s} = d\left(z + \frac{T_s}{A_s E_s}\right) \tag{53}$$

Thus, for p_{min}

$$W_1 = d\left(z + \frac{S_s}{E_s}\right) \tag{54}$$

W_2 for wire mesh may be computed from the same Eq. 48 as used for deformed bars in view of the fact that this value is generally very small in comparison with W_1.

Example

For a comparative study of crack behavior with deformed bars and wire mesh, consider the following numerical values (reduced physical constants for concrete are used, inasmuch as shrinkage is assumed to take place before the concrete reaches its full strength

value): S_s = 50,000 psi (assumed the same for bars and mesh); d = 20 in.; E_s = 30 x 10^6 psi; z = 2 x 10^{-4}; n = 10; E_c = 3 + 10^6 psi; S'_c = 100 psi; t = 8 in.; u = 400 psi; and A = 96 sq in.

From Eq. 33 p_{min} is computed as 0.00182. It should be noted that this is the same for both bars and wires. Selecting No. 4 deformed bars at 13½-in. centers results in Σ_0 = 1.35 sq in. and A_s = 0.175 sq in. For the mesh, 6/0 longitudinal wires and 1/0 transverse wires are selected.

From Vetter's equation (Eq. 19) L for deformed bars is computed as 5.54 ft. From Eq. 38, W_1 for deformed bars is computed as 0.0114 in.

For wire mesh, L is computed from Eq. 34 as 18.4 ft and W_2 from Eq. 54 as 0.0372 in. It may be noted, however, that if the transverse wire spacing is assumed as 6 in. instead of 20 in., the crack width and spacing are about the same as for deformed bars.

A comparison thus reveals that deformed bars tend to cause cracking at closer intervals, with less crack width resulting, and with the crack width being about proportional to the crack spacing. A narrow crack is desirable, as it protects the steel better and provides better aggregate interlock. However, the crack spacing and crack opening may be directly controlled in mesh by adjusting the distance between transverse wires. Closer spacing of transverse wires means closer crack spacing and smaller crack openings.

A numerical check of the value W_2 shows this to be negligible (less than 0.001 in.), and it may thus for practical purposes be ignored. This example problem is not intended to be used as a design criterion, but is presented simply to show the use of the basic equations.

BUCKLING TENDENCY

The phenomenon of blow-ups, or buckling, is well known in standard concrete pavements. It is the purpose of this investigation, therefore, to determine under what conditions buckling may occur in continuously-reinforced pavements. The condition of buckling is shown in Figure 9, in which

s = weight of slab per unit of surface;

F = the incipient buckling force per unit of width; and

M = the bending moment at x = 0 and x = l.

The differential equation of buckling behavior is

$$\frac{d^2y}{dx^2} = -\frac{M_x}{D_r} \tag{55}$$

where D_r is the reduced slab rigidity, defined by Eq. 14. From equilibrium, the bending moment at any distance, x, is

$$M_x = Fy - M + \frac{wx^2}{2} - \frac{wlx}{2} \tag{56}$$

Thus,

$$\frac{d^2y}{dx^2} + \frac{Fy}{D_r} = \frac{M}{D_r} + \frac{wlx}{2D_r} - \frac{wx^2}{2D_r} \tag{57}$$

The general solution to Eq. 57 is

$$y = A\cos kx + B\sin kx + \frac{M}{k^2 D_r} + \frac{w}{k^4 D_r} + \frac{wlx}{2k^2 D_r} - \frac{wx^2}{2k^2 D_r} \tag{58}$$

in which

$$k^2 = \frac{F}{D_r} \tag{59}$$

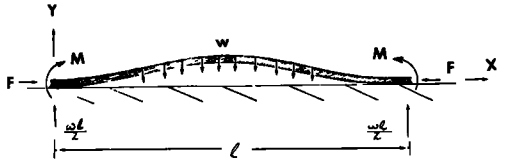

Figure 9. Slab buckling.

To evaluate the unknowns A, B, M, and F, four conditions are needed, as follows:

$(y)_{x=0} = 0$ (a)

$(y)_{x=l} = 0$ (b)

$\left(\frac{dy}{dx}\right)_{x=0} = 0$ (c)

$\left(\frac{dy}{dx}\right)_{x=l} = 0$ (d)

Boundary conditions (a) through (d) are then substituted in Eq. 58 or its first derivative. The following four equations are then obtained:

From (a),

$$A + \frac{M}{k^2 D_r} + \frac{w}{k^4 D_r} = 0 \tag{60}$$

From (b),

$$A \cos k l + B \sin k l + \frac{M}{k^2 D_r} + \frac{w}{k^4 D_r} = 0 \tag{61}$$

From (c),

$$B k + \frac{w l}{2 k^2 D_r} = 0 \tag{62}$$

From (d),

$$B k \cos k l - A k \sin k l - \frac{w l}{2 k^2 D_r} = 0 \tag{63}$$

To solve these four transcendental equations simultaneously to obtain k as a function of l, the first several terms of the Maclauren series are substituted for the sine and cosine functions.

$$\sin k l = k l - \frac{k^3 l^3}{6} + \cdots\cdots \tag{64}$$

$$\cos k l = 1 - \frac{k^2 l^2}{2} + \frac{k^4 l^4}{24} - \cdots\cdots \tag{65}$$

Upon the successive operations of substitution, simultaneous solution of the equations, and reduction, the following relation of k to l results:

$$k^2 = \frac{36}{l^2} \tag{66}$$

But from Eq. 59

$$k^2 = \frac{F}{D_r} = \frac{36}{l^2} \tag{67}$$

The incipient buckling force is thus

$$F = \frac{36 D_r}{l^2} \tag{68}$$

It should be noted that the incipient buckling force calculated from Eq. 68 is very nearly equal to Euler's classical critical buckling force for clamped ends and without any lateral force such as the slab weight,

$$F_{cr} = \frac{4\pi^2 D_r}{l^2} \tag{69}$$

If sufficient terms in the Maclauren expansion for the sine and cosine functions were taken, the incipient slab buckling force would be exactly equal to Euler's force. This thus indicates that the weight of the slab has no influence on the buckling force for the slab. Further proof of this is that the unit weight w cancels out in the preceding analysis.

There is, however, a very special and important limitation imposed on continuous pavements, not generally encountered in other buckling problems. This is the fact that the effective ends (where the assumed shapes as shown in Figure 9 meet the ground) are constrained against motion in the x direction by virtue of continuity. It is this fact that prevents actual uplift, despite the preceding analysis which indicates a possibility of incipient buckling.

To visualize the mechanics of actual buckling, consider that there first exists a sufficient axial force on the slab such that the slab is in a state of incipient buckling, given in this case by Eq. 69. If the ends of the slab were free to move under this force, the slab would indeed buckle upward, as in normal buckling action. However, due to the restrained ends, as soon as the slab tends to uplift as shown in Figure 9, the true length of the slab changes from the flat length to the longer length along the curve. Because the force F is imposed internally, as it would be by temperature or volume change in the concrete, this increase in length relieves that force. With F now decreased, the incipient buckling force is no longer materialized and the slab never actually uplifts.

For external forces greater than F, the slab may theoretically uplift slightly; but the uplift occurs gradually and over a very long length, such that the uplift is not visually observable. Furthermore, the uplift occurs gradually, and does not suddenly buckle.

Field observations[1] have verified this conclusion. In all the continuously-reinforced pavements built in the United States, no visible buckling has ever been recorded or observed, even when expansive forces have been large enough to cause compression failure and spalling at the terminal ends of the pavement (18).

MOVEMENT ON HORIZONTAL CURVES

It is conceivable that a roadway may change in horizontal alignment around a curve when a continuous slab of steel and concrete contracts or expands. The tendency to shorten or lengthen may cause the pavement at a curve to move inward or outward in the radial direction.

The simple calculation to follow establishes the conditions under which such movement would take place. It is the subgrade frictional drag which tends to prevent this radial movement. Consider a contraction tendency as shown in Figure 10. (Expansion would lead to the same general conclusion.)

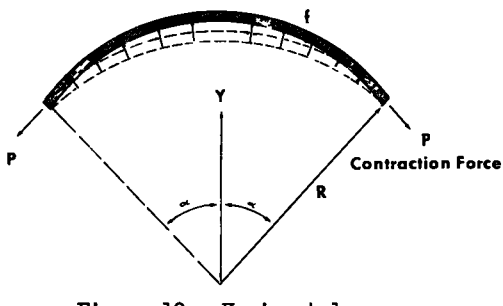

Figure 10. Horizontal curve.

The limiting subgrade drag force f per unit length of slab before appreciable radial movement may take place is μW, where μ is the coefficient of subgrade drag and W is the weight of pavement per unit length of slab.

From equilibrium of forces in the Y direction,

$$2 \mu W R \sin \alpha - 2 P \sin \alpha = 0 \tag{70}$$

From which it is found that the minimum radius that a roadway should have to prevent horizontal alignment changes is

[1] Confirmed in conversation with H. D. Cashell.

$$R_{limit} = \frac{P}{\mu W} \tag{71}$$

For cracked slabs, the limiting value of P may be taken as the total area of steel A'_s times the elastic limit of steel S_s.
Thus,

$$R_{limit} = \frac{A'_s S_s}{\mu W} = \frac{A_s S_s}{\mu w} \tag{72}$$

in which A_s is the area of steel per unit width and w is the weight of slab per unit of surface.

Considering a numerical example with $A_s = 0.5$ sq in. per ft, $S_s = 50,000$ psi, $w = 75$ psi, and $\mu = 1.5$, R_{limit} is computed from Eq. 72 to be 222 ft. Inasmuch as this radius is well below the normal radius used in highway design, it may be generally concluded that horizontal movements at curves are not a problem.

MOVEMENT ON VERTICAL CURVES

There exists the possibility that a continuous pavement on a vertical curve at the crest of a hill could tend to uplift from its base if sufficient concrete swelling due to moisture penetration and high temperature were to take place. Likewise, at a vertical curve at the bottom of a hill a tendency to uplift would be present if sufficient concrete shrinkage and temperature contraction existed. To investigate these possibilities the following analysis is presented.

Consider the contraction case shown in Figure 11 for a small ratio of h to a. Let ΔT be the total unrestrained contraction due to temperature and ΔS be the total unrestrained contraction due to shrinkage. Under the combined action of ΔT and ΔS the slab will tend to shorten and thus tend to lift off the ground. In doing this, there will be a force F induced throughout the slab caused by the weight of the slab. The exact "shape" of the slab would then be described by a catenary; however, to use a simpler (and almost exact) expression, the parabolic shape is assumed. Thus:

$$F = w a \sqrt{1 + \frac{a^2}{4 h^2}} \tag{73}$$

This force F then causes the slab to stretch a total length of $F l / A E$.

When this stretch $F l / A E$ equals $\Delta T + \Delta S$, the slab is recontacted with the base and the induced F thus vanishes. The resulting performance of the slab is as if it were simply straight and horizontal.

The criteria of uplift may then be expressed by

$$\Delta T + \Delta S > \frac{w a l}{A E} \sqrt{1 + \frac{a^2}{4 h^2}} \tag{74}$$

For cracked slabs in tension, A may be taken as A_s and E may be taken as E_s.

The behavior of a vertical curve in expansion at the crest of a hill is similar. It is only necessary to modify Eq. 74 by first considering ΔT as the total temperature expansion and ΔS as the total swelling expansion due to moisture and then, because the slab is in compression, all cracks in the concrete close up and

$$A = A_s + \frac{E_c}{E_s} A_c \tag{75}$$

and E should be taken as E_s. (This simply uses the transformed area properties of the concrete.)

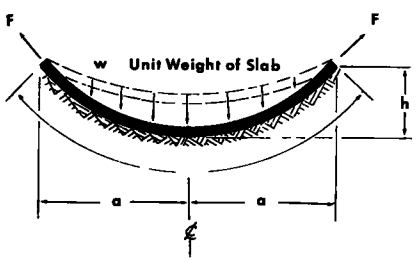

Figure 11. Vertical curve.

Example

Consider the following values for contraction: temperature drop = 80 F,

coefficient of expansion $\alpha = 0.0000075$ per degree F, a = 3,000 in., h = 100 in., E_s = 30×10^6 psi, w = 0.5 lb per in. (6-in. slab), $A_s = 0.0417$ psi, and $\Delta S = 0$. Thus, $\Delta T + \Delta S$ may be computed to be 3.7 in.; and

$$\frac{w a l}{A_s E_s} \sqrt{1 + \frac{a^2}{4 h^2}}$$

is computed to be 109 in. if the steel is assumed to remain elastic. From Eq. 74 it is thus obvious that there is no danger of uplift.

A comparative check on expansion for a temperature rise of 80 F, $\Delta S = 0$, and with all other values as for contraction, shows $\Delta T + \Delta S = 3.7$ in. and

$$\frac{w a}{\left(A_s + \frac{E_c}{E_s} A_c\right) E_s} \sqrt{1 + \frac{a^2}{4 h^2}} = 7.2 \text{ in.}$$

It should be noted that, due to the added action of the concrete, the deformation caused by the force F in compression is less than for tension. Nevertheless, from Eq. 74 it is clear that no uplift will take place in either case.

TERMINAL ANCHORAGE CONFIGURATION STUDIES

In the construction of existing continuously-reinforced roads, various types of end joints have been tried. Some consist only of standard filler strips as used in normal construction, whereas others are more elaborate, employing such joints as bridge-type expansion joints. Most of these have eventually proven unsatisfactory under service conditions; terminal movements of as much as 4 in. have been observed, resulting in damage to the pavement in the vicinity of the joint. As a possible alternate solution to these troublesome ends, it is suggested that the ends may be anchored instead of allowed to undulate. Several experimental anchors are being planned for a section of continuously-reinforced pavement to be built in southern Virginia. To study this problem a pilot model study was initiated by the Virginia Council of Highway Investigation and Research to determine the best anchorage configuration.

The test bed was dry sand, 2 ft by 14 ft upon which a wooden board (to which anchors were fastened) was placed as shown in Figure 12. The scale factor was 1/24 ft so that

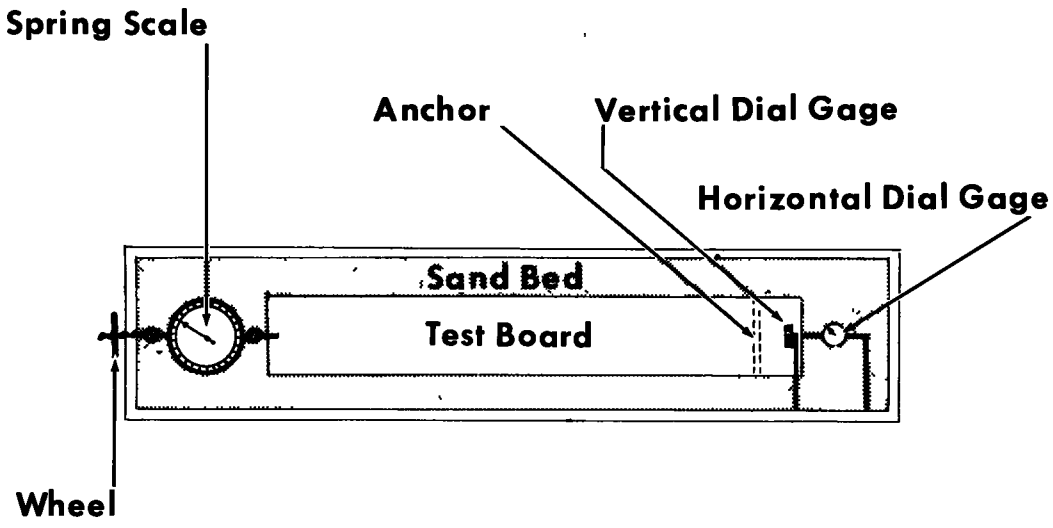

Figure 12. Test bed and apparatus.

the 12-in. by 12-ft board represented the terminal portion of road 24 ft wide and 288 ft long. It was not intended that this pilot study simulate the actual forces and movements at the end of a real slab; it was intended only to offer a qualitative comparison of anchorage resistances. On continuously-reinforced pavements only the last 300 ft or so have been found to move, therefore it is this portion which must be anchored. The anchorage configurations tested are those shown in Figure 13.

These shapes were varied in size, depth, and spacing, to observe relationships. The horizontal strength of this type of anchorage depends on the shape of the failure surface developed. Consider the action of an anchor such as shown in Figure 13a.

It is seen from Figure 14 that, due to the vertical restraining forces exerted by the slab on the soil acting as a surcharge, the failure surface is spread out and thus becomes more effective than if such vertical forces were not present. This vertical restraint can be attributed to a number of factors, including the weight of the slab, the bending resistance of the slab, the weight of the anchor, and the vertical friction of the anchor. Thus, the greater these factors, the greater is the maximum horizontal force P.

It may also be observed from Figure 14 that when the vertical anchor wall moves, it will displace the soil vertically, even allowing for consolidation. Thus, some uplift tendency can be expected. The more the failure surface is spread out due to the surcharge, the less will be the uplift. For a rough approximation in the limiting case of no surcharge, the vertical movement is about the same as the horizontal movement. With surcharge, the vertical movement is much less. The pilot tests have verified this.

Although load-versus-horizontal and vertical movement curves were obtained on all tests, it is felt that because these values were based only on a model study, their quantitative values are not as important as their relative values. Therefore, only a few sample curves are shown in Figure 15.

The important conclusions drawn from these tests may be summarized as follows:

Strength

Consider first a comparison of configurations a, b, and c (Figure 18), which are categorized as single solid anchorages. Taking a as a reference, it is found that due to the added confining action on soil by the side walls of the anchor, extra strength may be attained for the same projected area. Shape b is 14 percent stronger than a and shape c is 55 percent stronger than a. Shape f is also a single anchor, but consists of separated anchors. This shape produces the same strength as shape a for the same depth of embedment, despite the fact that the projected area is only 39 percent that of a. This may be accounted for in view of what happens to the failure surface as described in Figure 14. For a straight solid anchor such as a, the failure surface is essentially two-dimensional; but for an anchor such as in g, the soil flows not only in the direction of pull, but also transversely, creating a much larger three-dimensional failure surface. This thus results in the pile shapes having a much larger resistance than indicated merely by their projected area.

A second comparison may be made on the basis of depth of anchorage. For a given anchorage shape such as a the strength appears to vary linearly with depth, within the range of depths tested.

A third comparison may be made on multiple anchorages as in shapes d, e, and g.

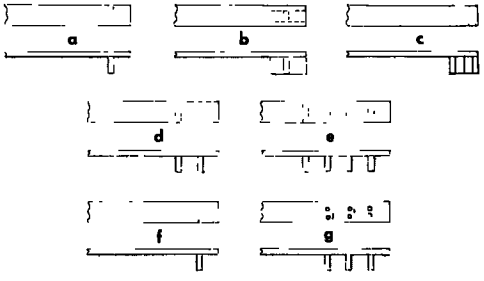

Figure 13. Anchorage configurations.

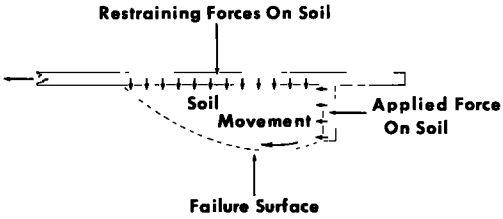

Figure 14. Failure surface.

A series of tests run on shape d with the spacing varying between anchors shows, as might be expected, that if the anchors are too close there is interference of action between the two and the full strength of both of them cannot be realized. It was found that for a scale-model distance of 48 in., or a prototype distance of 96 ft, the interference vanishes, and the full strength of each may be attained. The model depth for this test was 2 in., representing a prototype depth of 4 ft.

The over-all best performance in strength was attained by configuration g, which consists of a series of separated piles. For the same number and size of piles as f, g produced a strength 71 percent greater than f or a.

Uplift

As previously discussed, the problem of uplift is associated with strength. Two important conclusions seem to stand out after consideration of the test results. The first is that a distributed multiple anchorage, such as e or g, produces less uplift than a single large anchorage such as a, b, or c. This is understandable, as the load is more distributed and also the bending resistance of the pavement at interior positions is greater than at the end, allowing less vertical movement.

The second conclusion is that there is less uplift for the deeper anchors. This is also understandable, as a deeper anchor has more weight and more side frictional surface. Incidental to side friction, it was also found that the pile-shaped anchor f produced less uplift than a solid shape like a. This is partly explained by side friction and partly by the fact that the failure surface is three-dimensional, spreading the displaced soil over a larger area.

A comparison of uplift values, again taking shape a as a reference, shows that the uplift in a is 40 percent of the magnitude of the horizontal movement, whereas the uplift

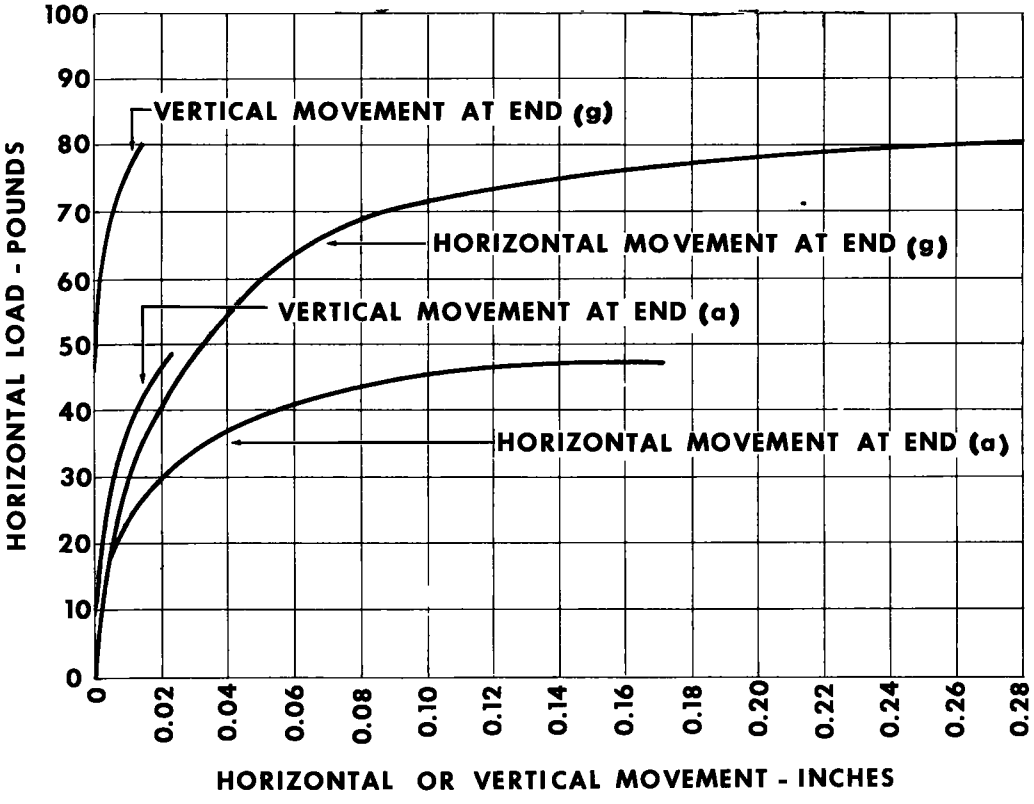

31a

Figure 15. Load-Movement curves for anchorage configuration as in Figure (12 A) and (12 g) (4" Model Depth).

in g is only 11 percent of the horizontal movement just prior to failure (see Fig. 15). In addition, the absolute vertical movement in g for corresponding loads is only about 25 percent of that for a, which shows the over-all superiority of g.

Therefore, as a general conclusion of comparison, it appears that a pile configuration such as Figure 12 g is the best for both maximum strength and minimum uplift.

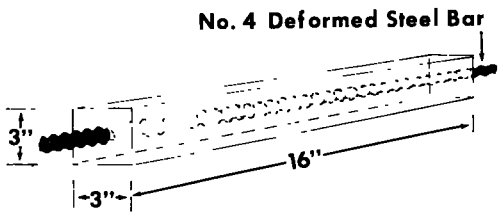

Figure 16. Test specimen.

Under actual field conditions it is believed that this shape could be quite economical if a truck-mounted earth augur bored holes into which a preassembled reinforcing steel cage could be placed. The holes could be monolithically filled with concrete at the same time the pavement is poured. A preliminary design indicates that about 10 such piles, 18 in. in diameter and 8 ft deep, could resist the terminal forces imposed by a continuously-reinforced pavement in either expansion or contraction.

When the full-scale anchorages are constructed on the proposed highway in southern Virginia, additional field observations will be taken on the horizontal and vertical movements, together with any other unusual cracking or behavior. More conclusive reports may be expected at that time.

CRACKED SLAB BEHAVIOR

As indicated earlier, in connection with the pavement thickness analysis and buckling analysis, there is need for information on the reduced bending rigidity of the slab in the longitudinal direction due to transverse cracking. To this end a pilot test program was conducted to obtain a behavioral trend.

Twenty test specimens (Fig. 16) were cast of concrete. After 28 days of moist curing, a concrete cylinder strength of 2,500 psi was reached. Each specimen was then artificially cracked by a pull on the steel bar sufficient to cause the concrete to crack transversely at various crack widths from 0.010 to 0.193 in. Several specimens were left uncracked to serve as a standard for comparison. The crack widths were measured with a calibrated microscope micrometer.

The specimens were then loaded transversely as beams, such as to cause a bending moment at the cracks of 1,440 in.-lb. This is within the standard allowable limit for normal concrete beams. Load-center deflection readings were then taken for the first, 10th, and 20th loading cycles. The load-deflection readings were not changed from the 10th to the 20th cycle.

Reduced Bending Rigidity

Figure 17 shows several typical load-deflection curves obtained. Note that these curves may be characterized in two stages. The small loads from 0 to about 350 lb are characterized by the fact that in this stage it is the flexing of the steel bar that is primarily controlling the bending of the beam, as the crack is still essentially open (see Fig. 18a). This is naturally a relatively weak phase. The second stage is that beyond 350 lb, where the concrete in compression acts in conjunction with the bending and axial tension in the steel, as shown in Figure 18b. This, or course, accounts for the rapid rise in strength as shown in Figure 17.

Based on the center deflection at the working load, a comparison of flexural rigidity may be made from the known elastic relation of load to deflection for a beam. The flexural rigidity is defined as EI, the modulus of elasticity times the effective moment of inertia. As used in the pavement thickness studies, the reduced rigidity is called D_r.

The plot of percentage of full uncracked rigidity and crack width is shown in Figure 19. Note that the flexural rigidity drops off rapidly with even small crack widths. Slabs with cracks of 0.20 in. have a rigidity of only 1 percent of that of an uncracked slab. The question of reduced rigidity as a function of crack spacing was not studied in this experiment.

Increase in Crack Width Under Repeated Loading

Field observations (12) of pavements in existence for many years have disclosed that lanes with more traffic have wider cracks than lanes with less traffic. This is clearly indicative of a condition resulting from repeated vehicular load, causing the cracks to flex back and forth under the bending moment imposed by the moving loads.

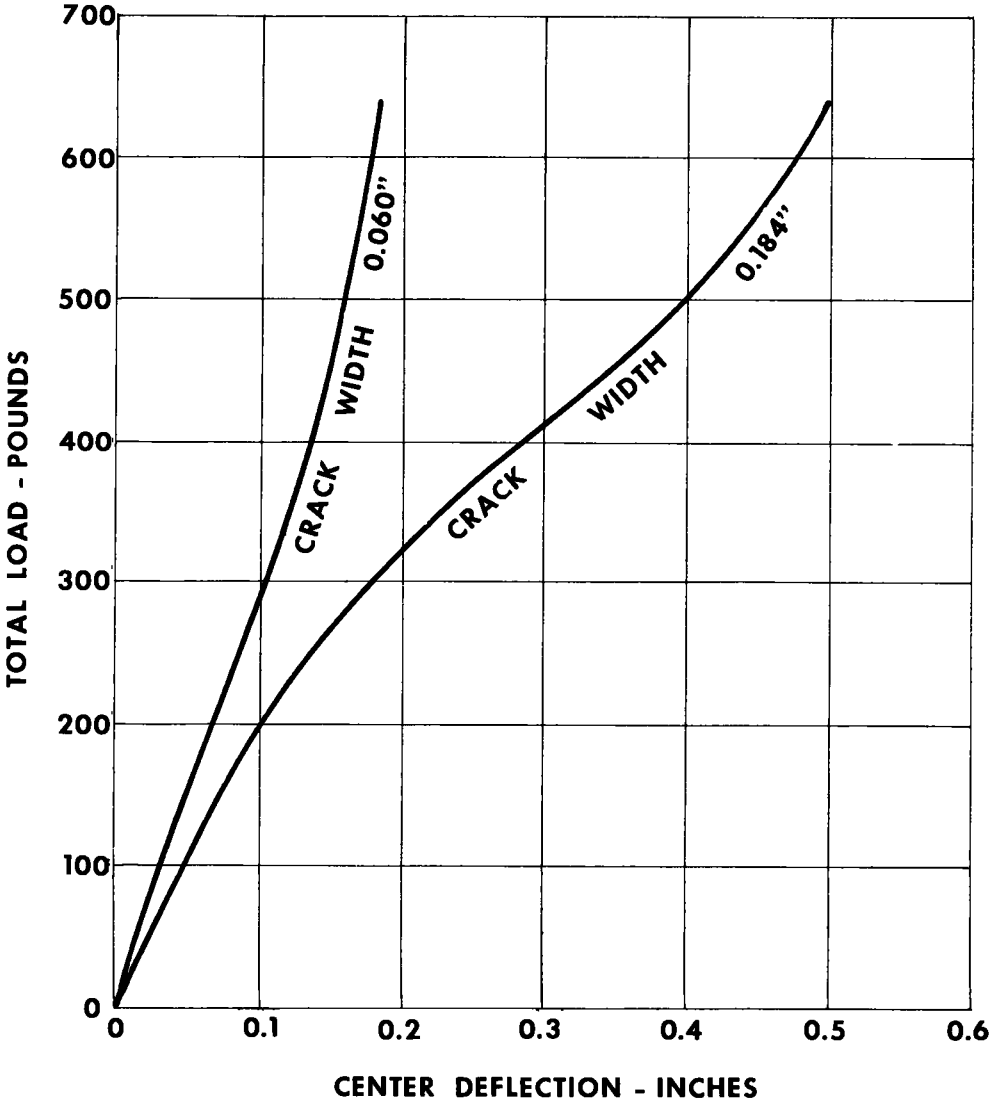

36 a

Figure 17. Typical load-deflection curves.

Figure 18. Crack behavior.

The same beam specimens and same apparatus set up to study crack width were used to determine the behavioral trend with repeated loadings. The loads were cycled from 0 to the full working load and back to 0 again. Average crack widths were taken after the 10th and 20th cycles. Only a

slight increase was noticed in the 20th cycle over the 10th cycle, so the results reported in Figure 20 are for 10 cycles. Note that although large percentage increases occur for small crack widths, this in reality still represents a very small real width of crack, because the percentage is based on an initially small value.

The increase in crack width under repeated loads is perhaps explained by a certain crushing and agitation of the cracked surfaces in the repeated flexing contact and recontact. For large cracks, this contact is confined to an area very near the surface, as shown in Figure 18b; in narrow cracks, the contact area is much greater. Because in this experiment only average crack widths were measured, the larger cracks did not reflect as much change as the smaller cracks.

Load repetition was not carried out far enough in this pilot study to cause fatigue failure. It is expected that fatigue failure would occur rapidly in the steel in the large crack widths for at least three reasons, as follows:

1. Large bending stresses occur in the steel bar itself, as discussed in connection with Figure 18.

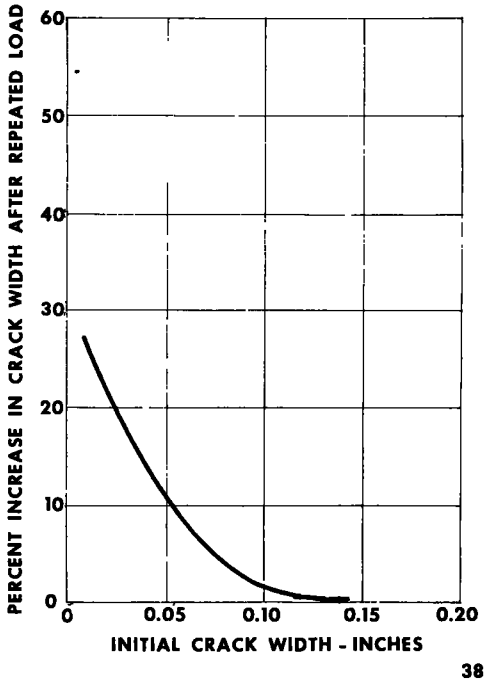

Figure 20. Increase in crack width after repeated loading.

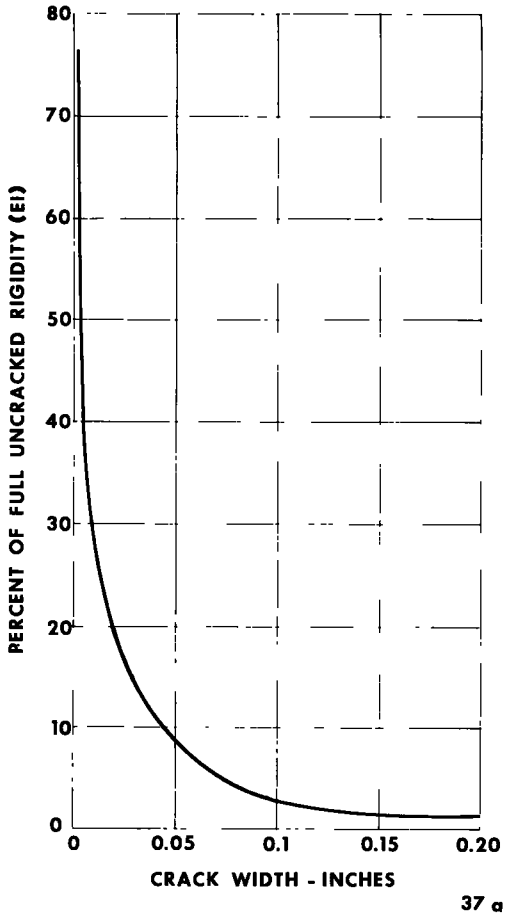

Figure 19. Reduction in rigidity.

2. The large crack results in the loss of aggregate interlock of the concrete, inducing high shear stresses in the steel.

3. Large cracks expose the steel to corrosion deterioration, which accelerates failure by fatigue.

These three reasons combine to cause early failure by fatigue. It is no surprise, therefore, that in all work in these tests and in this whole report, narrow crack widths are indeed the desirable object for the successful performance of a continuously-reinforced concrete pavement.

Because of the preliminary nature of this series of tests, coupled with the importance of information on repeated loads, it is highly desirable that additional test programs be conducted where the specimens are subjected to repeated loadings of many thousands of cycles. From several tests run incidental to the ones described, where the

loading was repeated 100 times, it appears that the crack width continues to enlarge. Repeated loading of many thousands of times on various strength concretes and various crack widths would thus reveal a more comprehensive behavior pattern.

ACKNOWLEDGMENTS

The work described in this report was done for the Virginia Council of Highway Investigation and Research under the direction of Tilton E. Shelburne, Director of Research. The writer wishes to express his thanks to Mr. Shelburne for the direction offered by his many years of experience in highway research and to L. R. Quarles, Dean of the School of Engineering, University of Virginia, for making possible the close cooperation between the Engineering School and the Research Council.

REFERENCES

1. Friberg, B. F., "Frictional Resistance Under Concrete Pavements and Restraint Stresses in Long Reinforced Slabs." HRB Proc., 33:170(1954).
2. Sutherland, E. C., and Benham, S. W., "Experiments with Continuous Reinforcement in Concrete Pavements." HRB Proc., 19:193(1939).
3. Cashell, H. D., and Benham, S. W., "Experiments with Continuous Reinforcement in Concrete Pavements." HRB Proc., 20:354(1940).
4. Cashell, H. D., and Benham, S. W., "Experiments with Continuous Reinforcement in Concrete Pavements: A Five Year History." HRB Proc., 23:35(1943).
5. Woolley, W. R., "Continuously Reinforced Concrete Pavements Without Joints." HRB Proc., 27:28(1947).
6. Russell, H. W., and Lindsay, J. D., "An Experimental Continuously Reinforced Concrete Pavement in Illinois." HRB Proc., 27:42(1947).
7. Van Breemen, W., "Preliminary Report of Current Experiment with Continuous Reinforcement in New Jersey." HRB Proc., 27:33(1947).
8. Cashell, H. D., and Benham, S. W., "Experiments with Continuous Reinforcement in Concrete Pavements." HRB Proc., 29:44(1949).
9. Russell, H. W. and Lindsay, J. D., "Three-Year Performance Report on Experimental Continuously-Reinforced Concrete Pavement in Illinois." HRB Proc., 30:45(1950).
10. Van Breemen, W., "Report on Experiment with Continuous Reinforcement in Concrete Pavement—New Jersey." HRB Proc., 30:61(1950).
11. Stanton, T. E., "Report on Experiment with Continuous Reinforcement in Concrete Pavements—California." HRB Proc., 30:28(1950).
12. Cashell, H. D., and Teske, W. E., "Continuous Reinforcement in Concrete Pavements." HRB Proc., 34:34(1955).
13. Vetter, C. P., "Stresses in Reinforced Concrete Due to Volume Changes." ASCE, 98:1039(1933).
14. Westergaard, H. M., "Computation of Stresses in Concrete Roads." HRB Proc., 5:90(1925).
15. Jacobs, W. H., "Continuously-Reinforced Concrete Pavements." Rail Steel Bar Assn. (1953).
16. Anderson, A. R., "Bond Properties of Welded Wire Fabrics." Proc., ACI, 48:681 (Apr. 1952).
17. Winter, G., "Stress Distribution in and Equivalent Width of Flanges of Wide, Thin-Wall Beams." N.A.C.A., TN 784 (1940).
18. Van Breemen, W. Private communication regarding a pavement in New Jersey.

Discussion

VEDAT YERLICI, Asst. Professor of Civil Engineering, Lehigh University, Bethlehem, Pa. — This paper contributes much to further understanding and knowledge of continuously-reinforced concrete highway pavements, and helps to clear up some doubtful points, such as buckling tendency and movement on horizontal and vertical curves. In certain respects it also raises questions.

Under the section on "Pavement Thickness" the slab is analyzed as a transverse beam between cracks. At the cracks the restraint is assumed to consist only of the upward reactions (shears) caused by the "elastic restraint of the adjacent segments transferred by the longitudinal steel" and by the "aggregate interlock". It would appear that the action of the cracked slab as a beam is somewhat questionable. If there is aggregate interlock at the crack there should also be twisting moments, which will reduce the deflections. Also, because there is considerable longitudinal steel, although not at the bottom of the slab, there also will be longitudinal moments. With all of these boundary conditions ignored, it is doubtful if this analysis fits the actual conditions better than the Westergaard theories, which do not assume cracks. Also, in the given differential equation of the beam on elastic foundations the aggregate interlock and the elastic restrain modulus are taken proportional to deflection. It is doubtful if these factors increase linearly with deflection; in the case of aggregate interlock even the reverse might be true.

If there is to be a rigorous mathematical analysis of the pavement, a section between cracks must be assumed partially restrained by shears, by longitudinal and torsional (twisting) moments at the cracked end, and free at the sides, and it should be analyzed as a plate over an elastic foundation. As this solution will be too complicated and time consuming, probably the whole pavement may be analyzed as an infinite or semi-infinite orthotropic plate strip on elastic foundation. In this analysis the effect of transverse cracks may be taken care of by assuming a reduced longitudinal rigidity for the pavement. On the other hand, it must be remembered that the item under consideration is a continuous, cracked, reinforced concrete slab resting on soil and that it is subjected to dynamic concentrated loads. The magnitudes of crack spacing and impact cannot be determined with certainty, and the modulus of elasticity, moment of inertia of reinforced concrete, and foundation modulus of any subbase, are not reliable factors. Therefore, at its best, this sort of analysis, based on such doubtful assumptions, cannot be much more than a help for a qualitative understanding of pavement behavior.

In comparing the behavior between the slabs reinforced with deformed bars and plain wire mesh, to simplify the matter, only the behavior in connection with shrinkage of concrete is discussed. When concrete is at the state of shrinking, its tensile and bond strengths are not fully developed and most probably the steel cannot restrain much of the contraction of concrete because of considerable slippage due to weakness of bond. At this stage the cracks will form mostly due to poor strength of concrete and frictional resistance between the subgrade and the pavement. Later, as the concrete cures, the influence of reinforcement as a crack former increases to be the major effect. Also, mechanical anchorages, such as the transverse bars of the wire mesh, may have an altogether different influence on the uncured concrete pavement than on the cured one. Hence, a study of the reinforcement influence that does not include the temperature effects on the cured pavement may give an incomplete picture and probably should not be generalized.

Anchoring the ends of the pavement, if it could be done cheaply, is a most constructive idea. It should present no problem when the slab is contracting, because the anchorage must only be stronger than the yield strength of steel; but the problem will get more complicated when the pavement expands, because of the high strength of concrete in compression. Thought also must be given to the possible plastic deformation, and creep, of the soil around the anchorages, because it may in time destroy the fixing effect of the anchors altogether.

WILLIAM ZUK, Closure — Most of Mr. Yerlici's comments are well considered and correct from a rigorous point of view, so that there is little to refute from this standpoint. However, he, as well as others, undoubtedly is aware that the simplifications and approach used were instituted not out of ignorance of the factors he mentioned, but in order to achieve a simplified workable design solution to some of the problems encountered in continuously-reinforced pavements. Some rational method of design is needed to replace the "rule of thumb" method now used.

Theoretical, laboratory, and field studies on various controversial phases of this subject are still being continued and it is hoped that eventually answers satisfactory to everyone will be found.